Also shown in Fig. 9 is the linear solution for a 5° pitch displacement. A considerable difference between the linear solution and the nonlinear solution for the payload pitch angle is apparent. For a similar one-degree displacement, the two solutions agree within ±0.04°.

Conclusions

Equations of motion that describe the three-dimensional motion of a nonrigid parachute and payload have been derived in a form which is convenient for numerical solution. A computer-aided small-disturbance stability analysis of the equations revealed that a relatively small parachute could be used to stabilize a statically unstable payload. Stability of the system was found to be improved by increasing parachute tangent force coefficient and normal force coefficient slope. Increasing riser length and parachute weight was seen to decrease system stability. The computer techniques developed allow a rapid stability analysis of large systems of linear ordinary differential equations of the type considered.

References

[1] Henn, H., "Descent Characteristics of Parachutes," R.A.E. Translation 233 of German Rept. ZWB/UM/6202, Oct. 1944, Royal Aircraft Establishment, Farnborough, England.

[2] Brown, W. D., *Parachutes*, Pitman and Sons Ltd., London, 1951.

[3] Lester, W. G. S., "A Note on the Theory of Parachute Stability," TN Mechanical Engineering 358, July 1962, Royal Aircraft Establishment, Farnborough, England.

[4] Heinrich, H. G. and Rust, L. W., "Dynamic Stability of a Parachute Point-Mass Load System," FDL-TDR-64-126, Air Force Flight Dynamics Lab., June 1965, Wright-Patterson Air Force Base, Ohio.

[5] Ludwig, R. and Heins, W., "Theoretical Studies of the Dynamic Stability of Parachutes," translated from the German by Faraday Translations, New York, Nov. 1964.

[6] White, F. M. and Wolf, D. F., "A Theory of Three-Dimensional Parachute Stability," *Journal of Aircraft*, Vol. 5, No. 1, Jan.-Feb. 1968, pp. 86–92.

[7] Heinrich, H. G. and Rust, L. W., "Dynamic Stability of a System Consisting of a Stable Parachute and an Unstable Load," AFFDL-TR-64-194, 1965, Air Force Flight Dynamics Lab., Wright-Patterson, Air Force Base, Ohio.

[8] Neustadt, M. et. al., "A Parachute Recovery System Dynamic Analysis," *Journal of Spacecraft and Rockets*, Vol. 4, No. 3, March 1967, pp. 321–326.

[9] Etkin, B., *Dynamics of Flight*, Wiley, New York, 1959.

[10] Ibrahim, S. K., "Experimental Determination of the Apparent Moment of Inertia of Parachutes," FDL-TDR-64-153, April 1965, Air Force Flight Dynamics Lab., Wright-Patterson Air Force Base, Ohio.

[11] "System/360 Scientific Subroutine Package," (360A-CM-03X) Version III, *Programmers Manual*, IBM H20-0205-3, 4th ed., 1968.

[12] Wolf, D. F., "The Dynamic Stability of Nonrigid Parachute and Payload System," Ph.D. thesis, 1968, Univ. of Rhode Island, Kingston, R.I.

AUGUST 1971 J. AIRCRAFT VOL. 8, NO. 8

Unsteady Airfoil Stall, Review and Extension

LARS E. ERICSSON* AND J. PETER READING†
Lockheed Missiles & Space Company, Sunnyvale, Calif.

A review of existing theoretical and experimental data has revealed that existing capabilities to predict full-scale unsteady airfoil stall are highly unsatisfactory. Existing theories can realistically only be applied to thin airfoil stall, and are completely inadequate in describing unsteady stall of the leading-edge or tailing-edge type, which comprise the stall types usually encountered both on helicopter rotors and compressor blades. The characteristic missing in present theories, and which completely dominates dynamic stall of the leading-edge and trailing-edge types, is the effect of pitch-rate-induced accelerated flow on the leeward side of a pitching airfoil. This flow acceleration produces a relief of the adversity of the pressure gradient, causing the observed delay of the stall and large overshoot of $C_{L_{max}}$. An analysis is presented that realistically describes unsteady airfoil stall in incompressible flow, including the accelerated flow effect on leading-edge and trailing-edge stall. It is found that quasi-steady theory, in which time history effects are lumped to one discrete past time event and the accelerated flow effect is represented by an equivalent time lag, can adequately describe the unsteady airfoil characteristics in the complete angle of attack range from substall into deep stall. Analytic predictions are found to agree well with dynamic experimental data. At very high frequencies, however, the agreement starts to deteriorate.

Nomenclature

AR = aspect ratio, $AR = b^2/S$
A/A_o = amplitude ratio, Eq. (2)
B/B_o = amplitude ratio, Eqs. (7–10)
b = wing span, m
C = general aerodynamic coefficient, Eqs. (1–3)
$c,\bar{c}$ = reference length, m: c = 2-dimensional chord length; $\bar{c} = S/b$, mean aerodynamic chord
f = frequency, cps
h = airfoil camber, m
L = lift, kg, coefficient $C_L = L/(\rho_\infty U_\infty^2/2)S$
l = lift, kg/m, coefficient $c_l = l/(\rho_\infty U_\infty^2/2)c$
M = Mach number
M_p = pitching moment, kg-m, $C_m = M_p/(\rho_\infty U_\infty^2/2)S\bar{c}$
m_p = pitching moment, kg-m/m, coefficient $c_m = m_p/(\rho_\infty U_\infty^2/2)c^2$
N = normal force, kg, coefficient $C_N = N/(\rho_\infty U_\infty^2/2)S$

Presented as Paper 70-77 at the AIAA 8th Aerospace Sciences Meeting, New York, January 19–21, 1970; submitted February 27, 1970, revision received November 19, 1970. The results were obtained in a study made for NASA Langley Research Center, Contract NAS 1-7999, under the direction of P. Hanson.

* Senior Staff Engineer. Associate Fellow AIAA.
† Research Specialist. Member AIAA.

n = normal force, kg/m, coefficient $c_n = n/(\rho_\infty U_\infty^2/2)c$
p = static pressure, kg/m^2, coefficient $C_p = (p - p_\infty)/(\rho_\infty U_\infty^2/2)$
q = pitch rate, rad/sec
$R_c, R_{\bar{c}}$ = Reynolds number based on chord length
S = reference area, m^2
t = time, sec
U = velocity, m/sec
x = horizontal coordinate, m
$z_{c.g.}$ = translatory coordinate, m (Fig. 3)
α = angle of attack, rad or deg
$\bar{\alpha}$ = generalized angle of attack, rad or deg, Eq. (4)
α_o = trim angle of attack, rad or deg (Fig. 3)
$\alpha(q)$ = pitch rate induced angle of attack, rad or deg (Fig. 3)
$\alpha(\dot{z})$ = translation induced angle of attack, rad or deg (Fig. 3)
Δ = increment
ϵ = downwash factor, Eq. (1)
ζ = dimensionless coordinate $\zeta = z_{c.g.}/c$ (Fig. 3)
θ = angle-of-attack perturbation, rad or deg (Fig. 3)
ξ = dimensionless x coordinate, $\xi = x/c$ (Fig. 3)
ξ_o = center of oscillation (Fig. 3)
ρ = air density, kg-sec^2/m^4
$\sigma(q)$ = pitch rate induced camber angle, rad or deg (Fig. 3)
Γ = airfoil circulation, m^2/sec (Fig. 1)
ϕ = phase lag, rad or deg Eq. (2)
$\Delta\phi$ = wake lag, rad or deg Eq. (2)
ψ = total phase angle, rad or deg Eqs. (7–10)
ω = oscillation frequency, rad/sec
$\bar{\omega}$ = reduced frequency, $\bar{\omega} = \omega\bar{c}/U_\infty$ or $\omega c/U_\infty$
ν = translatory phase angle, rad or deg Eq. (5)

Subscripts

a = accelerated flow effect
c.g. = center of gravity
e = boundary-layer edge conditions
s, stall = stall
w = wake lag effect
∞ = undisturbed flow
o = oscillation center and trim angle

Superscripts

$+$ = upstroke value
$-$ = downstroke value

Differential symbols

$\dot{\theta}$ = $\partial\theta/\partial t$
$\ddot{\zeta}$ = $\partial^2\zeta/\partial t^2$
C_{L_α} = $\partial C_L/\partial\alpha$
ϵ_α = $\partial\epsilon/\partial\alpha$

Introduction

UNSTEADY airfoil stall is an old problem that recently has received renewed attention by the compressor[1] and helicopter[2] industries. It is well documented experimentally that dynamic instability results when the airfoil penetrates into the stall region.[3,4] The resulting stall problems for helicopters have been enumerated recently.[5] Thus it is of great practical interest to be able to understand and predict unsteady airfoil stall characteristics. This is particularly so in view of the fact that even dynamically scaled model tests may not be applicable to full scale. The usual problems of wind tunnel and support interference are aggravated by the sensitivity of airfoil stall to surface roughness, flow uniformity, Reynolds number, and air turbulence. Only if the unsteady stall mechanism is fully understood can an "analytic extrapolation" to full scale be made with confidence.

It is clear that neither theory nor experiments alone will provide a satisfactory solution. However, if the unsteady aerodynamics can be related theoretically to static aerodynamic characteristics, which are readily available for a great number of airfoil shapes, a very substantial advancement of the state of the art will be accomplished. This has been attempted before without outstanding success. The present approach rests heavily on previously developed unsteady flow concepts for separated flow on launch vehicles[6] and re-entry bodies.[7] A conceptual flow picture is constructed and analytic relationships between dynamic and static characteristics are developed.

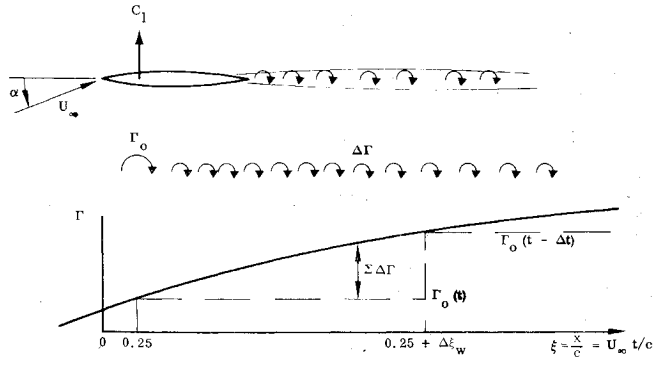

Fig. 1 The von Kármán-Sears vortex wake effects.

Analysis

The unsteady airfoil characteristics in incompressible flow will be derived using quasi-steady theory in which the time history is represented by one discrete past time event and the accelerated flow effect is represented by an equivalent time lag.

Below Stall

Below stall the classic treatment by von Kármán and Sears[8] will be used as the exact theory with which to compare quasi-steady time-lagged theory. In the von Kármán-Sears theory, the effect of the airfoil wake is represented by a continuous vortex sheet with the vorticity related to the in-

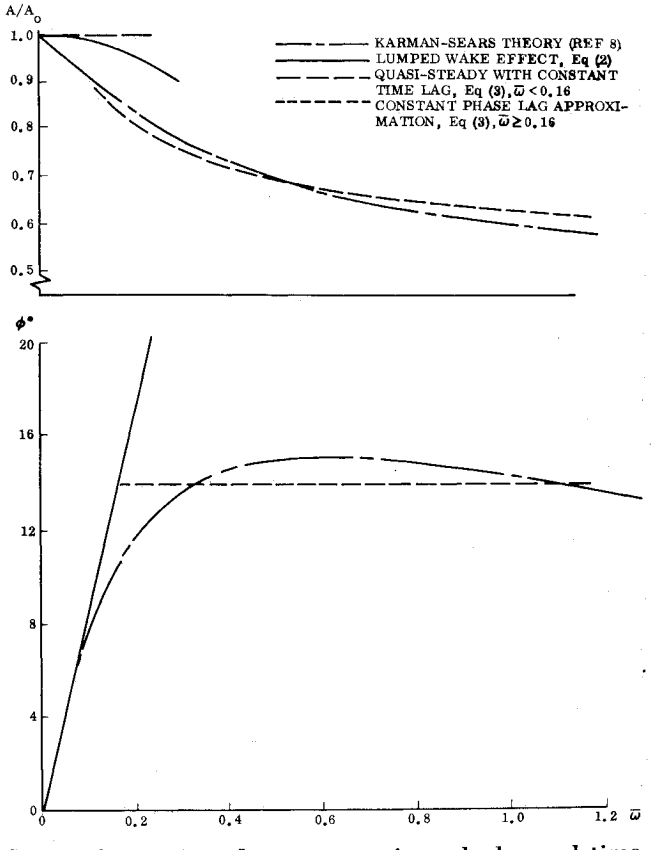

Fig. 2 Comparison between quasi-steady lumped-time history treatment and exact theory for vortex wake effects below stall.

stantaneous variation of the "lifting-surface" vorticity over the airfoil at earlier time instants. In Fig. 1, the "lifting-surface" vorticity distribution is represented by the lifting line vortex Γ_o at 25% chord with the requirement of zero velocity normal to the airfoil at 75% chord, a "lumped vorticity" representation that has been in frequent use since Multhopp[9] proposed it. It is immediately apparent that the downwash from unit size vortex elements between $\xi = 0.25$ and $\xi = 1.25$ would give zero net downwash at 75% chord. If the reduced frequency is low, one can expect that the effect of the continuous vortex wake can be approximated by one discrete "spilled" vortex (located downstream of $\xi = 1.25$). The strength of this vortex is the difference between the strength of the lifting line vortex at an earlier time instant $\Gamma_0(t - \Delta t)$, and its present strength, $\Gamma_o(t)$.

In the von Kármán-Sears theory the mutual interference between vortex elements is neglected and the vortices are assumed not to move relative to their environment, i.e., they are transported downstream relative to the airfoil with freestream velocity. Thus, the unsteady characteristic of the airfoil can be written

$$C(t) = C(\alpha_o) + C_\alpha\{\theta(t) - \epsilon_\alpha[\theta(t) - \theta(t - \Delta t)]\} \quad (1)$$

where $\Delta t = c(\xi - 0.25)/U_\infty = c\Delta\xi_w/U_\infty$.

For harmonic oscillations $\alpha(t) = \alpha_o + \Delta\theta \sin\omega t$ the corresponding variation of the airfoil characteristic can be written

$$[C(t) - C(\alpha_0)]/(C_\alpha\Delta\theta) = (A/A_o)\sin(\omega t - \phi) \quad (2a)$$

$$A/A_0 = \{[1 - \epsilon_\alpha(1 - \cos\Delta\phi)]^2 + [\epsilon_\alpha \sin\Delta\phi]^2\}^{1/2} \quad (2b)$$

$$\phi = \arctan\{(\epsilon_\alpha \sin\Delta\phi)/[1 - \epsilon_\alpha(1 - \cos\Delta\phi)]\} \quad (2c)$$

$$\Delta\phi = \omega\Delta t = \bar{\omega}\Delta\xi_w \quad (2d)$$

The results obtained by von Kármán-Sears[8] suggest the following values on ϵ_α and $\Delta\xi_w$ in Eq. (1): $\epsilon_\alpha = 0.5$; $\Delta\xi_w = 3$.

At low frequencies this quasi-steady lumped time history theory compares well with the von Kármán-Sears theory (Fig. 2). The results suggest the following approximation for the unsteady vortex-wake effect (also shown in Fig. 2).

$$C(t) - C(\alpha_o) = C_\alpha\Delta\theta\,(A/A_o)\sin(\omega t - \phi) \quad (3a)$$

$$\frac{A}{A_o} = \begin{cases} 1 & : \bar{\omega} < 0.16 \\ 0.475[1 + (10\bar{\omega})^{-1/2}]: & \bar{\omega} \geq 0.16 \end{cases} \quad (3b)$$

$$\phi = \begin{cases} 1.5\bar{\omega} & : \bar{\omega} < 0.16 \\ 14^\circ & : \bar{\omega} \geq 0.16 \end{cases} \quad (3c)$$

All generation of circulation-lift has this vortex-wake effect. An airfoil pitching around an oscillation center $\xi_{c.g.} = \xi_o$, that also describes translatory oscillations, has the following component characteristics:

$$C_L(t) - C_L(\alpha_o) = C_{L_\alpha}\{\tilde{\alpha}(t) - \epsilon_\alpha[\tilde{\alpha}(t) - \tilde{\alpha}(t - \Delta t)]\} + C_{L_\sigma}(\sigma[q(t)] - \epsilon_\alpha\{\sigma[q(t)] - \sigma[q(t - \Delta t)]\}) \quad (4a)$$

$$C_m(t) - C_m(\alpha_o) = C_{m_{o_\sigma}}([\sigma q(t)] - \epsilon_\alpha\{\sigma[q(t)] - \sigma[q(t - \Delta t)]\}) - [C_L(t) - C_L(\alpha_o)](0.25 - \xi_o) \quad (4b)$$

$$\tilde{\alpha}(t) = \theta(t) + \alpha[q(t)] + \alpha[\dot{z}(t)] \quad (4c)$$

$\theta,\alpha(q),\sigma(q)$, and $\alpha(\dot{z})$, as defined in Fig. 3, are

$$\theta(t) = \Delta\theta \sin\omega t \quad (5a)$$

$$\alpha[q(t)] = (0.5 - \xi_o)\bar{\omega}\Delta\theta \cos\omega t \quad (5b)$$

$$\sigma(q(t)) = \bar{\omega}\Delta\theta \cos\omega t \quad (5c)$$

$$\alpha[\dot{z}(t)] = \bar{\omega}\Delta\zeta \cos(\omega t + \nu) \quad (5d)$$

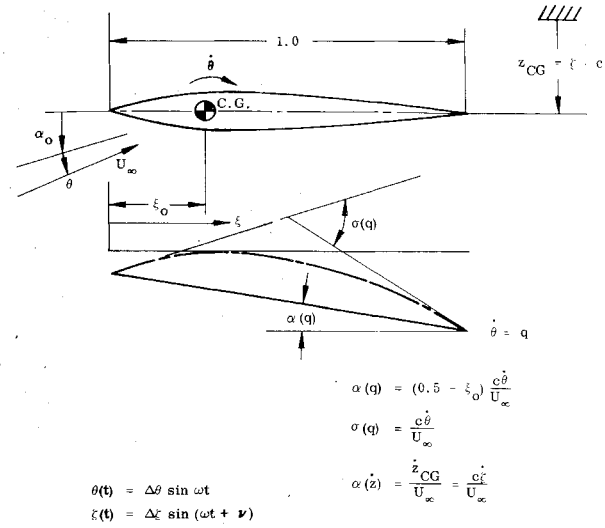

Fig. 3 Definitions of perturbations $\theta,\alpha(q),\sigma(q)$, and $\alpha(\dot{z})$.

In addition to these time lagged characteristics there are the instantaneous apparent mass effects[10]

$$C_L(\ddot{z}) = (\pi/2)(\bar{c}^2\ddot{\zeta}/U_\infty^2) \quad (6a)$$

$$C_m(\ddot{z}) = \pi/2(\xi_0 - 1/2)\bar{c}^2\ddot{\zeta}/U_\infty^2 \quad (6b)$$

$$C_L(\dot{\theta}) = (\pi/2)(\bar{c}\dot{\theta}/U_\infty) \quad (6c)$$

$$C_L(\ddot{\theta}) = -\pi/2(\xi o - 1/2)\bar{c}^2\ddot{\theta}/U_\infty^2 \quad (6d)$$

$$C_m(\dot{\theta}) = \pi/2(\xi o - 1/2)\bar{c}\dot{\theta}/U_\infty \quad (6e)$$

$$C_m(\ddot{\theta}) = -\pi/2[(\xi o - 1/2)^2 + 1/32]\bar{c}^2\ddot{\theta}/U_\infty^2 \quad (6f)$$

Two special cases are of particular interest, viz., pure translations and pure oscillations in pitch.

Translatory oscillations

$$z(t) = \bar{c}\Delta\zeta \sin\omega t \quad (7a)$$

$$C_L(t) - C_L(\alpha_o) = C_{L_\alpha}\bar{\omega}\Delta\zeta(B/B_o)\cos(\omega t - \psi) \quad (7b)$$

$$B/B_o = (A/A_o)\cos\phi[1 + (\tan\phi - a_1)^2]^{1/2} \quad (7c)$$

$$\tan\psi = \tan\phi - a_1 \quad (7d)$$

$$a_1 = [(\pi/2)\bar{\omega}/C_{L_\alpha}]/[(A/A_o)\cos\phi] \quad (7e)$$

$$C_m(t) - C_m(\alpha_o) = -C_{L_\alpha}\bar{\omega}\Delta\zeta(0.5 - \xi_o)(B/B_o)\cos(\omega t - \psi) \quad (8a)$$

$$B/B_o = (A/A_o)\cos\phi[a_2^2 + (a_2\tan\phi - a_1)^2]^{1/2} \quad (8b)$$

$$\tan\psi = \tan\phi - a_1/a_2 \quad (8c)$$

$$a_2 = (0.25 - \xi_o)/(0.50 - \xi_o) \quad (8d)$$

Pure oscillations in pitch: $\theta = \Delta\theta \sin\omega t$

$$C_L(t) - C_L(\alpha_o) = C_{L_\alpha}\Delta\theta(B/Bo)\cos(\omega t - \psi) \quad (9a)$$

$$B/Bo = (A/Ao)\cos\phi[(b_1 + a_1 - \tan\phi)^2 + (b_1\tan\phi + 1 - a_3)^2]^{1/2} \quad (9b)$$

$$\tan\psi = (b_1\tan\phi + 1 - a_3)/(b_1 + a_1 - \tan\phi) \quad (9c)$$

$$b_1 = (0.5 - \xi_o + C_{L_\sigma}/C_{L_\alpha})\bar{\omega} \quad (9d)$$

$$a_3 = a_1(0.5 - \xi_o)\bar{\omega} \quad (9e)$$

$$C_m(t) - C_m(\alpha_o) = -C_{L_\alpha}\Delta\theta(0.5 - \xi_o)(B/B_o)\cos(\omega t - \psi) \quad (10a)$$

$$B/B_o = (A/A_o)\cos\phi\{[(b_1a_2 - b_2) - a_2\tan\phi + a_1]^2 + [(b_1a_2 - b_2)\tan\phi + a_2 - a_4]^2\}^{1/2} \quad (10b)$$

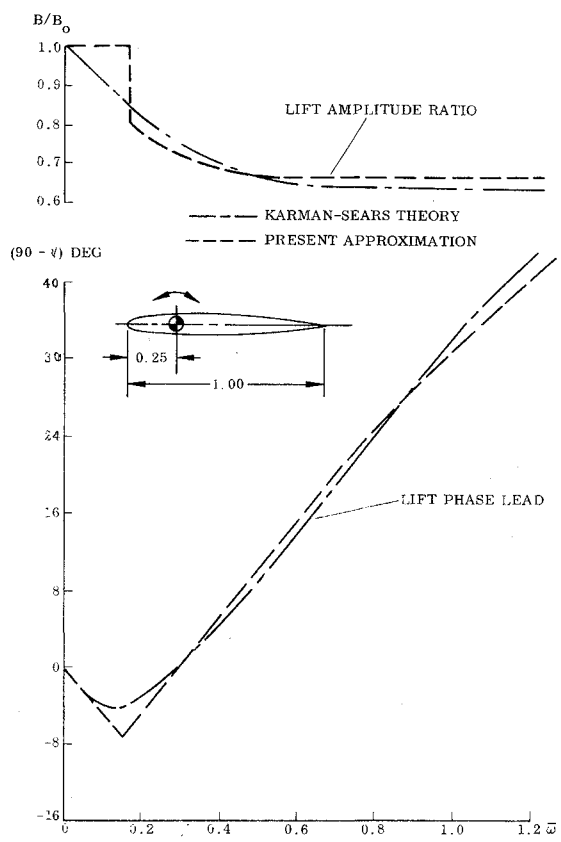

Fig. 4 Substall dynamic lift characteristics for small amplitude oscillations in pitch around quarter chord.

$$\tan\psi = [(b_1a_2 - b_2)\tan\phi + a_2 - a_4]/[(b_1a_2 - b_2) - a_2\tan\phi + a_1] \quad (10c)$$

$$b_2 = C_{m_{o_\sigma}}\bar{\omega}/C_{L_\alpha}(0.5 - \xi_o) \quad (10d)$$

$$a_4 = a_3 + a_1\bar{\omega}/32\ (0.5 - \xi_o) \quad (10e)$$

Equations (9) and (10) are illustrated in Figs. 4 and 5 for $\xi_o = 0.25$.

Stall Penetration

When and where separation occurs is determined by the boundary-layer profile shape and the adversity of the local pressure gradient. On the pitching airfoil, the flow acceleration on the leeward side will delay the flow separation. The pressure gradient of the external flow at the boundary-layer edge is given by the complete Bernoulli equation

$$-(1/\rho_e)(dp_e/dx) = \partial U_e/\partial t + U_e(\partial U_e/\partial x) \quad (11)$$

With $x/c = \xi$, Eq. (11) can be written

$$dp_e/d\xi = -\rho_e U_e[(\partial U_e/\partial t)(c/U_e) + \partial U_e/\partial\xi] \quad (12)$$

For constant freestream velocity, U_e changes only through airfoil pitching. Thus

$$dp_e/d\xi = -\rho_e U_e[(\partial U_e/\partial\alpha)(c\dot{\alpha}/U_e) + \partial U_e/\partial\xi] \quad (13)$$

That is

$$dp_e/\partial\xi = (\partial p_e/\partial\xi)_{\dot{\alpha}=0} + (\partial p_e/\partial\alpha)(c\dot{\alpha}/U_e) \quad (14)$$

On the leeward side of the airfoil $\partial p_e/\partial\alpha$ is negative, as suction increases with angle of attack. Consequently, the pressure gradient dp_e/dx is decreased on the leeward side when the airfoil pitches at a certain rate, $c\dot{\alpha}/U_e > 0$, and the boundary layer separation is, as a consequence, delayed.

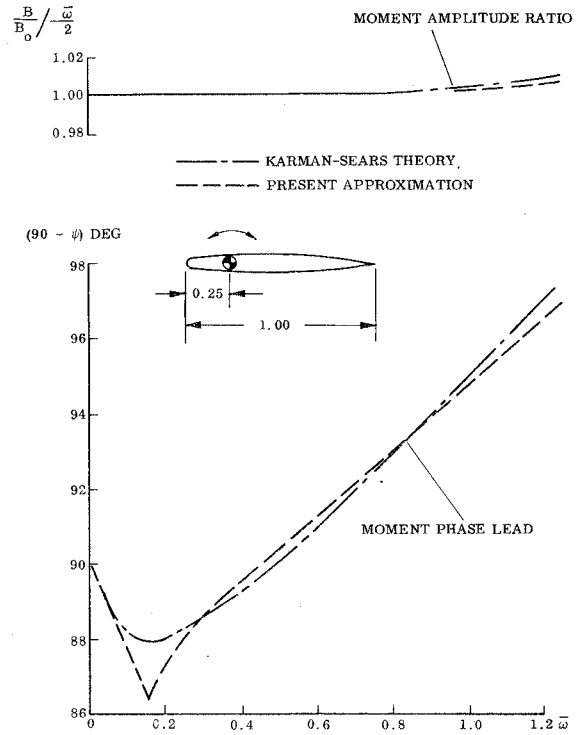

Fig. 5 Substall dynamic moment characteristics for small amplitude oscillations in pitch around quarter chord.

That is, the separation will in the unsteady case lag behind the static or steady-state condition, allowing an overshoot of the static stall angle of attack.

Discussion

Substantial overshoot of the static $C_{L_{max}}$ has been observed on aircraft penetrating the stall at non-zero angle-of-attack rates.[11,12] The overshoot of α_{stall} and corresponding overshoot of $C_{L_{max}}$ at low Mach numbers are almost entirely caused by the pitch rate induced flow acceleration and corresponding delay of the adversity of the leeward side pressure gradient, the "frequency induced plunging" described in Ref. 13. The decrease of the adversity of the pressure gradient is proportional to $(c\dot{\alpha}/U_\infty)$—see Eq. (14)—and the overshoot of the stall angle of attack will also be proportional to $(c\dot{\alpha}/U_\infty)$. For leading-edge type of stall, the α_s-overshoot $\Delta\alpha_s$ gives directly an overshoot of $C_{L_{max}}$, $\Delta C_{L_{max}} = C_{L_\alpha}\cdot\Delta\alpha_s$ (Fig. 6a). Similarly, an effective $\Delta\alpha_s$ can be defined for the $C_{L_{max}}$-overshoot of trailing-edge stall (Fig. 6b). The overshoot derivative $\partial\alpha_s/\partial(c\dot{\alpha}/U_\infty)$ can be used to define the overshoot $\Delta\alpha_s$ as follows:

$$\Delta\alpha_s = \frac{\partial\alpha_s}{\partial(c\dot{\alpha}/U_\infty)}\frac{c\dot{\alpha}}{U_\infty} = (\dot{\alpha})_{mean}\Delta t = \left(\frac{c\dot{\alpha}}{U_\infty}\right)_{mean}\Delta\xi_a \quad (15)$$

Thus, the overshoot derivative $\partial\alpha_s/[\partial(c\dot{\alpha}/U_\infty)]$ is equivalent to a dimensionless time lag $\Delta\xi_a$, where $\Delta\xi_a$ is the distance in chord lengths that the airfoil travels during the acceleration produced overshoot of α_s (and $C_{L_{max}}$). Experimental dynamic data give the following range for $\Delta\xi_a$; $1 < \Delta\xi_a < 9$. The large values of this equivalent time lag means that the dynamic effects of flow separation can be large even when the static effects are small. At higher subsonic speeds, the $C_{L_{max}}$-overshoot is negligible.[12] This does not, however, mean that the acceleration-induced effects are negligible. The shock-induced separation existing at higher Mach numbers induce a force couple very similar to that existing on cone cylinders at high subsonic Mach numbers.[14,15]

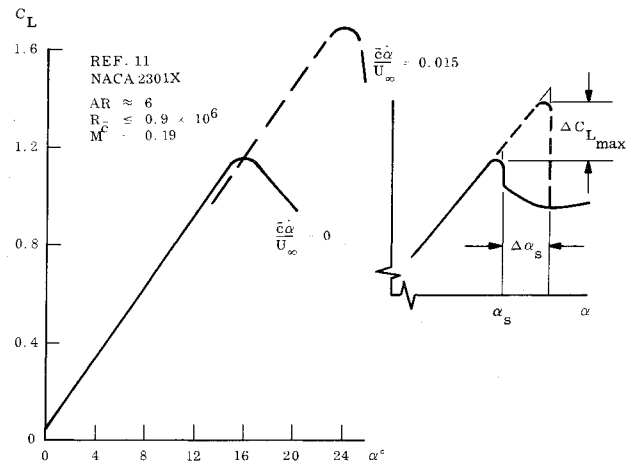

a) Leading-edge stall

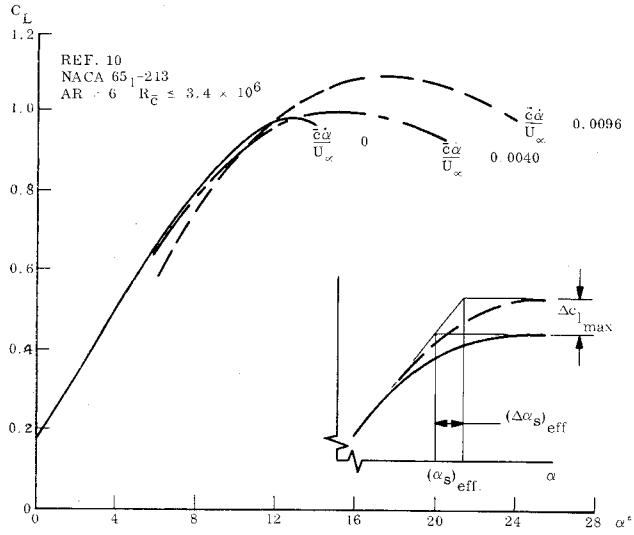

b) Trailing-edge stall

Fig. 6 $C_{L_{max}}$—overshoot characteristics.

On an oscillating airfoil the frequency induced plunging[13] causes a similar overshoot of the static stall. Oscillatory stall data[3] (Fig. 7) indicate that the equivalent time lag for the stall overshoot is $\Delta\xi_a = 2$. This magnitude is also obtained for dynamic stall of the trailing-edge type.[11,16] For leading-edge stall, moment stall precedes lift stall appreciably and is, therefore, a better indicator of the accelerated-flow-induced stall delay. Thus, the very high value of $\Delta\xi_a$ implied by Fig. 6 is largely due to post stall vortex interference effects.[16]

In order to predict unsteady airfoil characteristics vs instantaneous angle of attack (the loops presented by Carta, Liiva, Halfman, and others[1-3]) the graphical construction from static characteristics described in Ref. 13 is used. Figure 8 shows in detail how the construction is done. First, the instantaneous loop is constructed. This is a composite of effects which include lift overshoot and undershoot, and attached and separated flow camber effects. Attached flow phase lag (lumped von Kármán-Sears lag) is used below stall, where attached flow is anticipated, and the additional accelerated-flow-phase lag is added after static stall, i.e., for $\alpha(t) > \alpha_s$. The discontinuous change in phase lag at α_{stall} is faired out over $\Delta\alpha = 2°$.

For turbulent trailing-edge stall complete antisymmetry can be assumed for the delay of separation and reattachment caused by the accelerated flow effect on the adversity of the pressure gradient. The turbulent separation behavior is very similar to boundary-layer transition[17], i.e., the separation does not occur suddenly but is present down to low

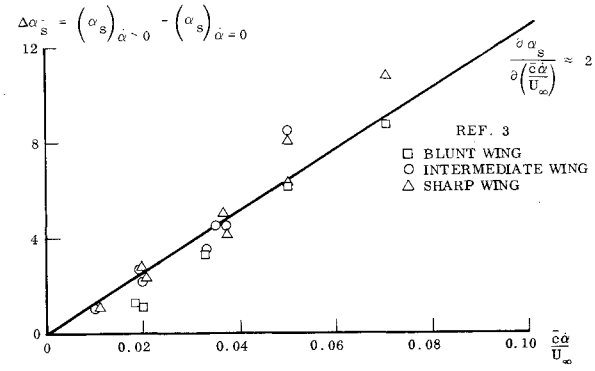

Fig. 7 Oscillatory data for dynamic stall overshoot.

adverse pressure gradients or low angles of attack in form of transitory stall spots that originate in the laminar sublayer. Thus, the gradual loss of lift can be thought of as a measure of the intermittency factor for turbulent stall. As the pressure gradient grows more and more adverse (with increasing α) the spots grow in number and size, start to coalesce, and finally destabilize the entire flow to develop full stall.

In constructing the instantaneous loop the limiting $C_{L_{max}}$ for infinitely large Reynolds numbers was used, as oscillatory stall data obtained by Halfman[3] and others indicate that the oscillating airfoil seems to have a very much higher turbulence level than the static airfoil.[16] The translating airfoil in Fig. 9

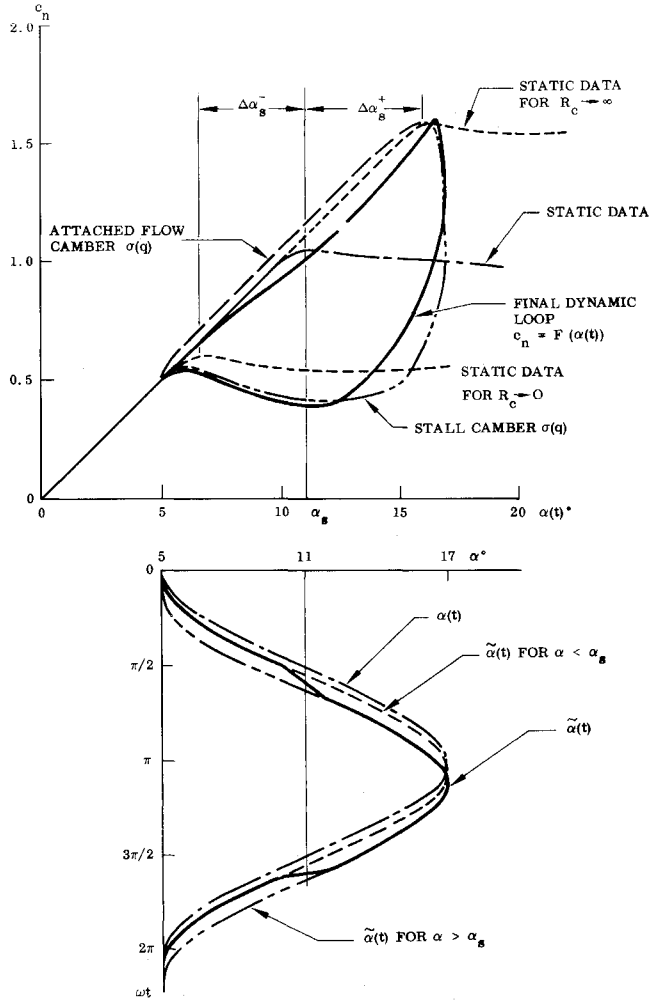

Fig. 8 Quasi-steady construction of dynamic normal force characteristics including time lag effects due to vortex wake and accelerated flow for turbulent trailing-edge stall.

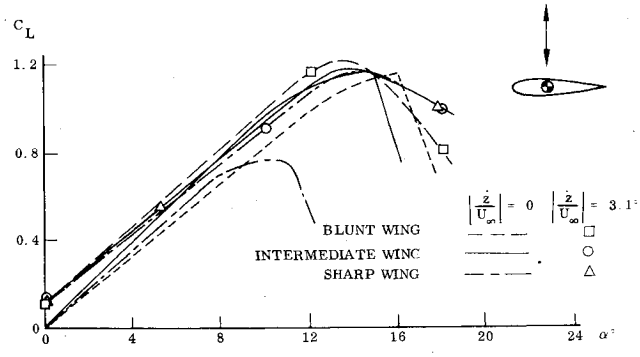

a) Translating airfoil

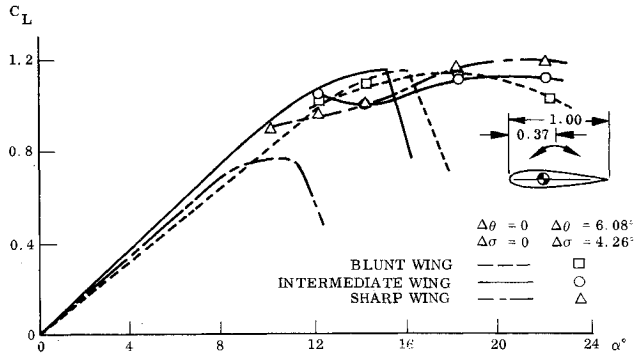

b) Pitching airfoil

Fig. 9 Comparison between time average $C_L(\alpha)$-curves for blunt, intermediate, and thin wings at $R_c = 10^6$ (Ref. 3).

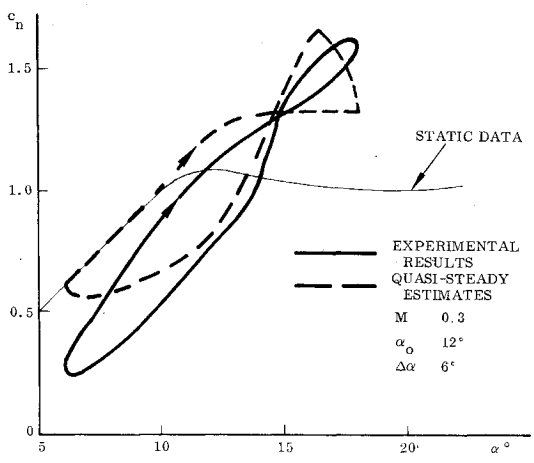

a) Low frequency ($\bar{\omega} = 0.15$)

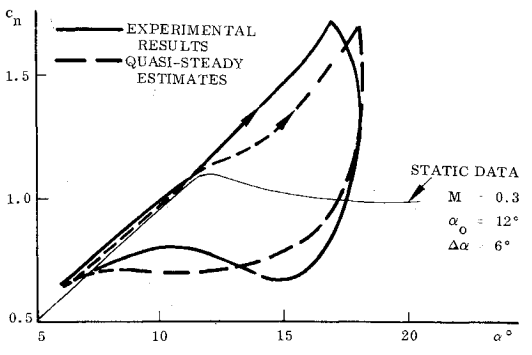

b) High frequency ($\bar{\omega} = 0.60$)

Fig. 10 Effect of frequency on normal force estimates for dynamic trailing-edge stall (NACA 0012 airfoil section, Ref. 1).

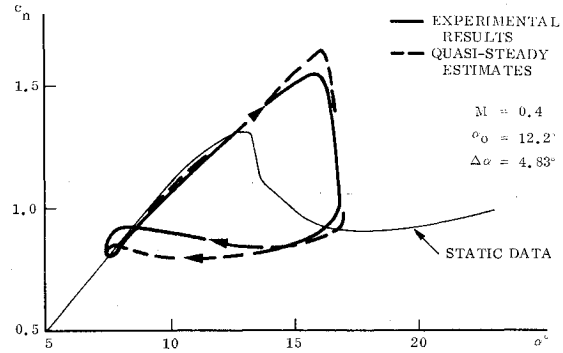

a) Low frequency ($\bar{\omega} = 0.15$)

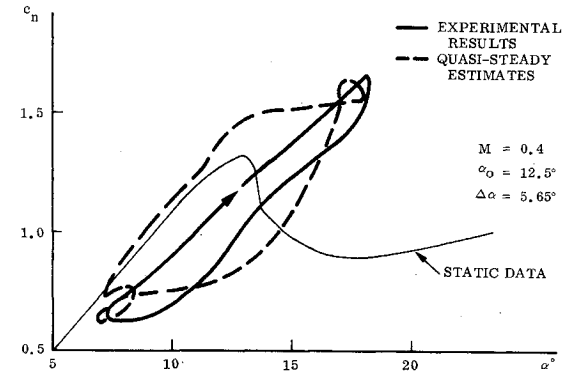

b) High frequency ($\bar{\omega} = 0.71$)

Fig. 11 Effect of frequency on normal force dynamic characteristics (VERTOL 23010-1.58 airfoil section, Ref. 2).

has not the large pitch rate induced accelerated flow effect, and one would expect the time average C_L to agree fairly well with the static C_L. This is true for the blunt and intermediate wing, but the sharp wing shows an unexpected large overshoot of static C_L. The only rational explanation we have been able to find is that the translatory oscillation generates a higher effective Reynolds number than the nominal $R_c = 10^6$, causing a large increase of $C_{L_{max}}$. It is the sharp wing, with its high nose curvature, that will benefit most from the energizing of the boundary layer (an effect possibly equivalent to an increase of effective Reynolds number), whereas the nose radius of the other two wings is large enough to make Reynolds number changes above $R_c = 10^6$ relatively less influentual on $C_{L_{max}}$. When the airfoil is oscillating in pitch, the increased accelerated-flow effect causes the expected additional overshoot. It is the fact that the three wings reach very much the same (limiting) $C_{L_{max}}$ characteristics that suggests using the limiting value for $R_c \to \infty$ to obtain the appropriate static characteristics to use for the "upstroke" in the unsteady analysis. Conversely, the limiting characteristics for $R_c \to 0$ are used for the reattachment characteristics.

According to the assumed antisymmetry of turbulent trailing-edge stall, $\Delta\xi_a$ is the same for the "down-stroke" as for the "upstroke." Thin airfoil theory or static experimental data gives the attached-flow pitch-rate-induced camber effect,[13] while static experimental data are used to obtain the effect of camber after separation. Separated-flow camber effects are used down to the stall point, $\alpha = \alpha_s - \Delta\alpha_s$, of the assumed static reattachment curve. At the limits of the cycle when $\dot{\alpha} = q = 0$, steady lift values are used. The appropriate attached-flow and separated-flow time lags described previously are then applied to these instantaneous characteristics to obtain the final dynamic loop. Throughout the loop constructions presented here, an effective equivalent time lag of $\Delta\xi_a = 2$ was used for the accelerated-flow effect, as it seemed to be a representative value for turbulent trailing-

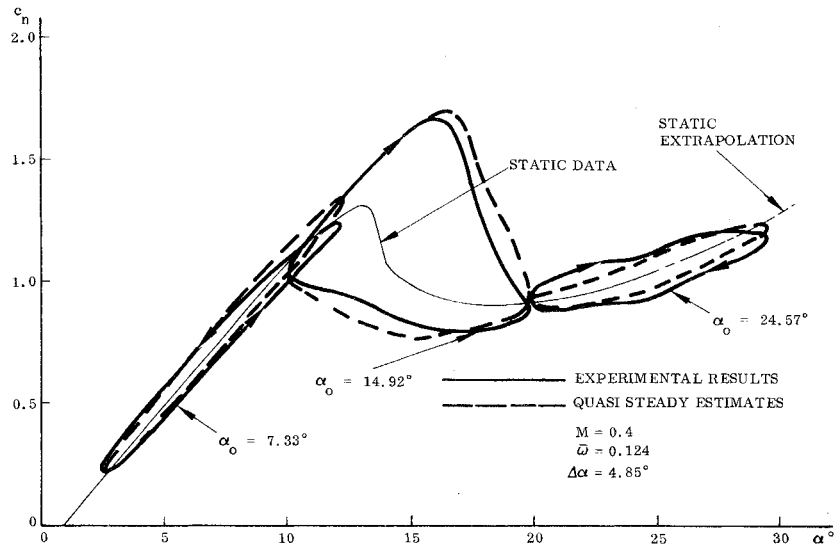

a) Normal force characteristics

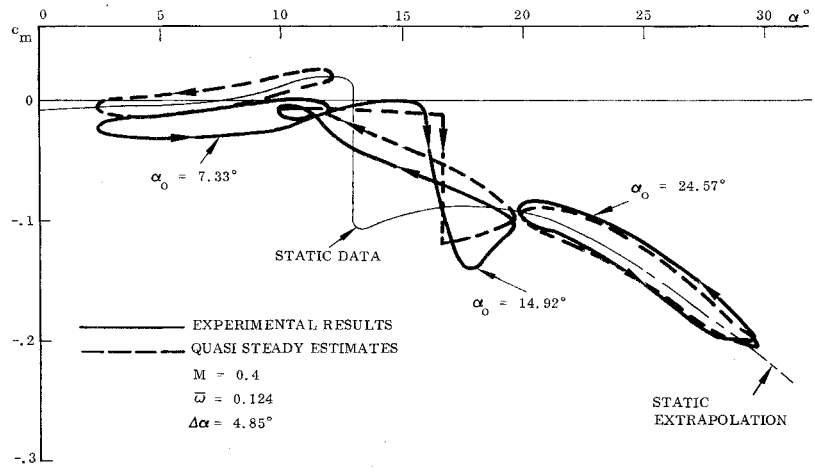

b) Pitching moment characteristics

Fig. 12 Effect of angle of attack on dynamic characteristics of VERTOL 23010-1.58 airfoil (Ref. 2).

edge stall. Dynamic data (Ref. 3 and Fig. 7) indicate this to be valid also for leading-edge stall, and both stall types are treated in the same manner when constructing the dynamic loops. For thin airfoil stall there may not be any accelerated-flow effects to be concerned about, and it appears that it should be possible to predict the unsteady characteristics by the methods proposed by Sarpkaya[18] and Ham.[19] No specific examples of unsteady thin airfoil stall are discussed in the present paper.

Figure 10 shows how well the quasi-steady time-lagged predictions agree with Carta's data for trailing-edge type stall.[1] Figure 11 shows that Liiva's data[2] also can be predicted with a fair amount of success. The effect of frequency is the same for both Carta's and Liiva's data. That is, at high frequencies the agreement between quasi-steady prediction and experimental data starts to deteriorate (Figs. 10b and 11b). At low frequencies, however, the measured dynamic characteristics are well predicted throughout the angle of attack region from sub-stall to deep stall (Fig. 12). It is especially encouraging that the moment characteristics are so well predicted, including the undamping loop obtained at stall penetration (Fig. 12b).

In view of all the various flow mechanisms involved, the success of the simple analytical predictions from static data to match the experimental dynamic characteristics is very encouraging. It is undoubtedly true, however, that much work still remains before the problem of dynamic stall will be completely understood. A more detailed knowledge of the static characteristics is needed, in particular, in regard to the transition from stall to reattachment. At high reduced frequencies, interaction with the "spilled" vortex for leading-edge stall[16] and with motion-independent vortex shedding have to be included, as well as downwash effects from the previous "stroke."

Conclusions

A study of unsteady airfoil stall has revealed that most of the apparently anomalous characteristics of trailing-edge and leading-edge stall can be explained by simple analytic concepts and can, to a large extent, be predicted from static (experimental) characteristics. The prominent and outstanding problem analytically is the large dynamic overshoot of static stall and undershoot of static reattachment.

The overshoot and undershoot are caused by two oscillation induced effects: 1) the effect of the induced flow acceleration on the adversity of the pressure gradient; and 2) the effect of the induced change of the effective Reynolds number or turbulence level. Both effects are to a first approximation proportional to $c\dot{\alpha}/U_\infty$ the dimensionless frequency-induced plunging.

The aforementioned general characteristics are often upset by a change of stall type. Thus, a static leading-edge stall may convert into a dynamic trailing-edge stall. This can happen through oscillation-induced accelerated-flow effects on the pressure gradient or by the oscillation-induced energizing

of the leading-edge boundary layer resulting in an apparent increase of the "effective Reynolds number."

References

[1] Carta, F. O., "Unsteady Normal Forces on an Airfoil in a Periodically Stalled Inlet Flow," *Journal of Aircraft*, Vol. 4, No. 5, Sept.-Oct. 1967, pp. 416–421.

[2] Liiva, J., "Unsteady Aerodynamic and Stall Effects on Helicopter Rotor Blade Airfoil Sections," *Journal of Aircraft*, Vol. 6, No. 1, Jan.-Feb. 1969, pp. 46–51.

[3] Halfman, R. L., Johnson, H. C., and Haley, S. M., "Evaluation of High-Angle-of-Attack Aerodynamic-Derivative Data and Stall-Flutter Prediction Techniques," TN 2533, 1951, NACA.

[4] Rainey, A. G., "Measurement of Aerodynamic Forces for Various Mean Angles of Attack of an Airfoil Oscillating in Pitch and on Two Finite-Span Wings Oscillating in Bending with Emphasis on Damping in the Stall," TN 3643, 1955, NACA.

[5] Harris, F. D., and Pruyn, R. P., "Blade Stall—Half Fact, Half Fiction," *American Helicopter Society Journal*, Vol. 13, No. 4, April 1968, pp. 27–48.

[6] Ericsson, L. E., and Reding, J. P., "Analysis of Flow Separation Effects of the Dynamics of a Large Space Booster," *Journal of Spacecraft and Rockets*, Vol. 2, No. 4, July-Aug. 1965, pp. 481–490.

[7] Ericsson, L. E. and Reding, J. P., "Dynamic Stability Problems Associated with Flare Stabilizers and Flap Controls," AIAA Paper 69-182, New York, Jan. 1969.

[8] von Kármán, T. and Sears, W. R., "Airfoil Theory for Non-Uniform Motion," *Journal of the Aerospace Sciences*, Vol. 5, No. 10, Aug. 1938, pp. 379–390.

[9] Multhopp, H., "Die Berechnung der Auftriebsverteilung von Trafluegeln," *Luftfahrt Forschung*, Bd. 15, 1938, p. 153.

[10] Lomax, H., Heaslet, M. A., Fuller, F. B., and Sluder, L., "Two and Three-Dimensional Unsteady Lift Problems in High-Speed Flight," Rept. 1077, 1952, T.R., p. 18.

[11] Conner, F., Willey, C., and Twomey, W., "A Flight and Wind Tunnel Investigation of the Effect of Angle-of-Attack Rate on Maximum Lift Coefficient," CR-321, 1965, NASA.

[12] Harper, P. W., and Flanigan, R. E., The Effect of Rate of Change of Angle of Attack on the Maximum Lift of a Small Model," TN 2061, 1949, NACA.

[13] Ericsson, L. E., "Comment on Unsteady Airfoil Stall," *Journal of Aircraft*, Vol. 4, No. 5, Sept.-Oct. 1967, pp. 478–480.

[14] Ericsson, L. E., "Loads Induced by Terminal-Shock Boundary-Layer Interaction on Cone-Cylinder Bodies," *Journal of Spacecraft and Rockets*, Vol. 7, No. 9, Sept. 1970, pp. 1106–1112.

[15] Ericsson, L. E., Aeroelastic Instability Caused by Slender Payloads," *Journal of Spacecraft and Rockets*, Vol. 4, No. 1, Jan. 1967, pp. 65–73.

[16] Ericsson, L. E., and Reding, J. P., "Unsteady Airfoil Stall," CR 66787, 1969, NASA.

[17] Kline, S. J., "Some New Concepts of the Mechanics of Stall in Turbulent Boundary Layers," *Journal of the Aerospace Sciences*, Vol. 24, No. 6, June 1957, pp. 470–471.

[18] Sarpkaya, T., "Separated Unsteady Flow About a Rotating Plate," *Proceedings of the Tenth Midwestern Mechanics Conference: Developments in Mechanics*, Vol. 4, 1968, pp. 1485–1499.

[19] Ham, N. D., "Aerodynamic Loading on a Two-Dimensional Airfoil during Dynamic Stall," *AIAA Journal*, Vol. 6, No. 10, Oct. 1968, pp. 1927–1934.

AUGUST 1971 J. AIRCRAFT VOL. 8, NO. 8

T-Tail Transport Empennage Loads in Continuous Atmospheric Turbulence

H. M. Dodd Jr.*
Sandia Laboratories, Albuquerque, N. Mex.

AND

K. G. Pratt†
NASA Langley Research Center, Hampton, Va.

Empennage loads on a T-tail transport were determined for simultaneous application of vertical and lateral gust components of atmospheric turbulence. A real-time analog-digital computer simulation employing data from tests in the NASA Langley transonic dynamics tunnel investigated the relative importance of nonlinear effects caused by the combined gusts. These effects were found to be negligible, but the linear contributions of the lateral gust on the horizontal stabilizer load were found to be significant. Results are presented in the form of power spectral densities and load exceedance rates that indicate how much the expected maximum stabilizer load is increased when combined gusts are considered.

Nomenclature

A = tail total angle of attack due to motion and gust for zero mean load
$\bar{A}$ = ratio of rms output response to rms gust input
a_y, a_z = lateral and vertical acceleration of a point on the empennage
B, BH = vertical tail and horizontal stabilizer total angles of sideslip due to motion and gust
$BM1,2,3$ = bending moments in horizontal stabilizer, fin tip, and fin root
b = span of wing
C_{ij} = nondimensional empennage load coefficient [see Eq. (10)]
$\bar{c}$ = wing mean aerodynamic chord
$d(\eta)$ = perpendicular distance from elemental mass location to bending moment axis
f_0 = natural frequency, Hz
f_{v_g}, f_{w_g} = lateral and vertical gust forces
H = complex one-dimensional frequency response function

Presented at the AIAA/ASME 11th Structures, Structural Dynamics, and Materials Conference, Denver, Colo., April 22–24, 1970 (no paper number; published in bound volume of conference papers); submitted June 5, 1970; revision received February 17, 1971. This work was conducted under NASA Research Grant NGR-17-002-047 to the University of Kansas.

* Member of the Technical Staff, Systems Environmental Testing Department.

† Aerospace Technologist, Aerodynamic Loads Branch, Loads Division. Member AIAA.